Supplementary Information for

Controlling the Charge of Single Nanoparticles in an Ion Trap

Sophia C. Leippe,[a] Kleopatra Papagrigoriou,[a] Carl Behrendt,[a] Björn Bastian*[a]

[a] Wilhelm Ostwald Institute for Physical and Theoretical Chemistry, Leipzig University, Linnéstraße 2, 04103 Leipzig, Germany

* Björn Bastian, Email: bjoern.bastian@uni-leipzig.de

S1 Trapped and measured nanoparticles in this study

Table S1. Measured NPs in this study: material, initial charge and mass, diameter and information on the type of experiment (varying buffer gas or trap settings). The initial charge was determined after trapping and pre-charging with the cold cathode gauge for stable trapping at 25 kHz trap frequency. The NP diameter is determined based on the initial mass, assuming a sphere with a bulk density of 2.65 g cm^{-3} for SiO_2 and 19.32 g cm^{-3} for Au. For NPs A–D, only the standard trap settings (sine waveform, 200 V) were applied.

NP	Material	Initial charge (e)	Initial Mass (MDa)	Diameter (nm)	Experiment
A	SiO_2	993	1822	130	Ar, N_2, O_2
B	SiO_2	388	1053	108	O_2, He
C	SiO_2	562	1592	124	Ar
D	SiO_2	572	1213	113	Ar, O_2
E	SiO_2	456	767	97	Ar, trap settings
F	SiO_2	1171	1718	127	Ar, trap settings
G	SiO_2	707	1661	126	Ar, trap settings
H	Au	562	928	53	Ar
J	Au	274	941	54	Ar

S2 Calculated probability of emitted charge carriers to reach the ion trap based on buffer gas collisions (without trap potentials)

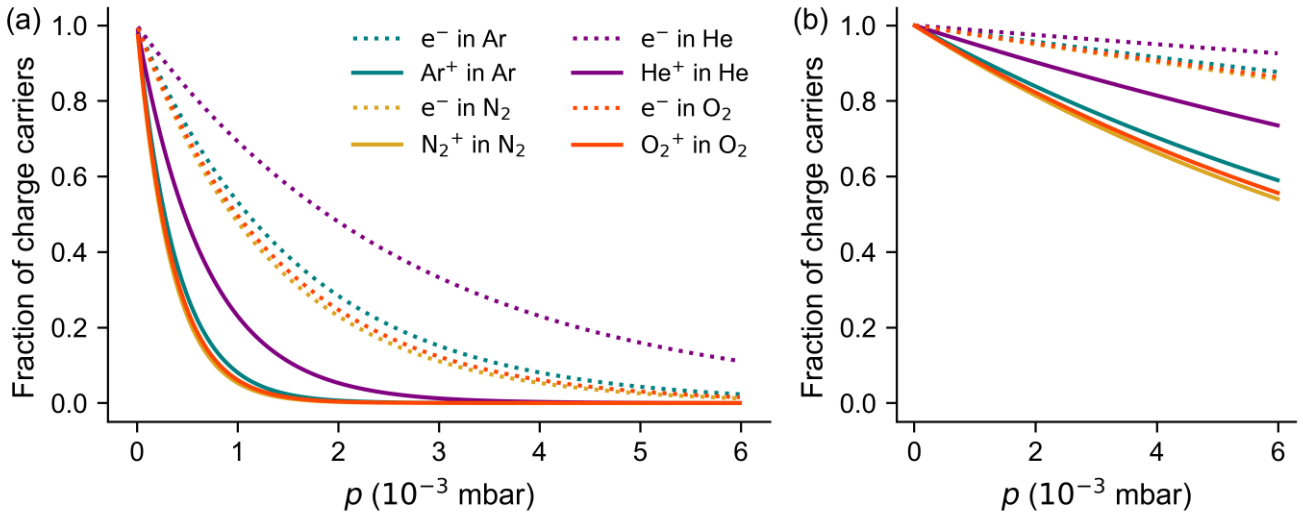

Figure S1. Calculated fractions of electrons (dotted) and gas cations (solid) that reach the trap center from (a) the cold cathode gauge (from which they are emitted) at a 20 cm distance and (b) from a 7 mm distance (see curly brace in Figure 7a) without colliding with other gas atoms, as a function of pressure p. The calculation is based on a distance d of 20 cm or 7 mm, the mean free path λ and the collision cross sections σ_{col}. The fraction of charge carriers (e.g. electrons e^-) that reach the trap center is $\mathrm{N}^{\mathrm{e}^-} / \mathrm{N}_0^{\mathrm{e}^-} = \exp\left(-\frac{\mathrm{d}}{\lambda}\right)$ with mean free path $\lambda = \frac{\mathrm{k_B T}}{\sqrt{2}\,\mathrm{p}\,\sigma_{\mathrm{col}}}$, Boltzmann constant $\mathrm{k_B}$, and temperature T. For gas cations, experimental cross sections $\sigma_{\mathrm{col,\ gas}}$ are used.[1] For electrons, the derived cross section is $\sigma_{\mathrm{col,\,e}} = \pi\left(\frac{1}{2}\sqrt{\sigma_{\mathrm{col,\ gas}}/\pi}\right)^2$, based on the relation $\sigma_{\mathrm{col,\,AB}} = \pi\,(\mathrm{r_A} + \mathrm{r_B})^2$.

S3 Aluminium foil to reduce charge carrier stream from wide-range gauge

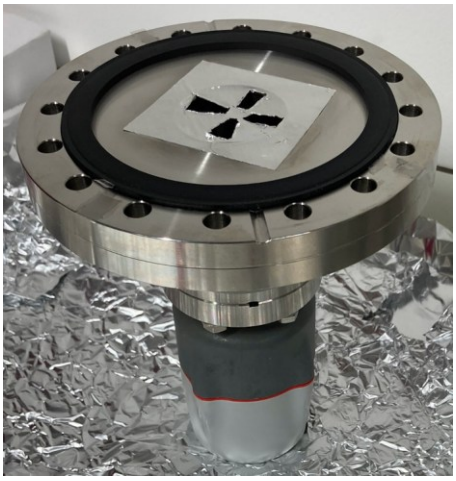

Figure S2. Dismounted flange on which an aluminum foil with cutouts is installed as well as the wide-range gauge that is used for NP charging. The aluminum foil reduces the stream of photons and charge carriers coming from the wide-range gauge region to the trap center.

S4 Pressure dependence of charge carriers in the ion trap

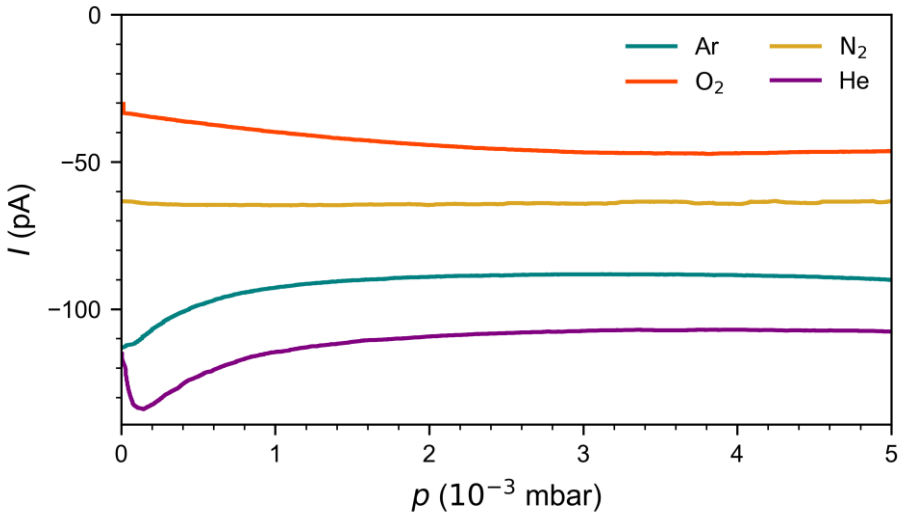

Figure S3. Negative electric current I as a function of pressure p. The current is a measure of the number of electrons and was measured on the ion trap electrode that is closest to the trap center. The pressure gauge was turned on, the trap potentials were inactive, and a positive bias potential (+ 90 V) was applied to the trap electrode to attract the electrons from the trap region.

S5 Simulated probability of charge carriers reaching the trap center

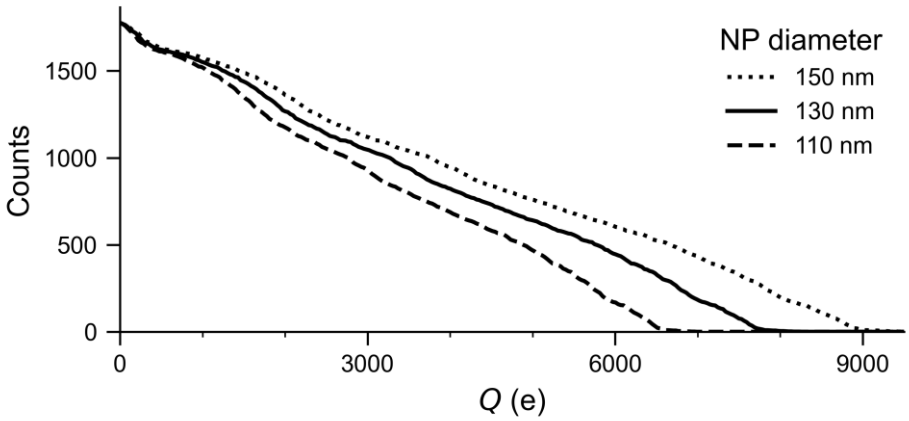

Figure S4. Simulated number of gas cations that have a kinetic energy high enough to overcome the Coulomb repulsion by a NP in the trap center, plotted against the NP charge Q for NP diameters specified in the legend. Ion start positions were drawn from a uniform distribution in the full trap volume of which less than 1% reach the trap center. Simulations were performed for a sine waveform with 200 V amplitude and 25 kHz frequency.

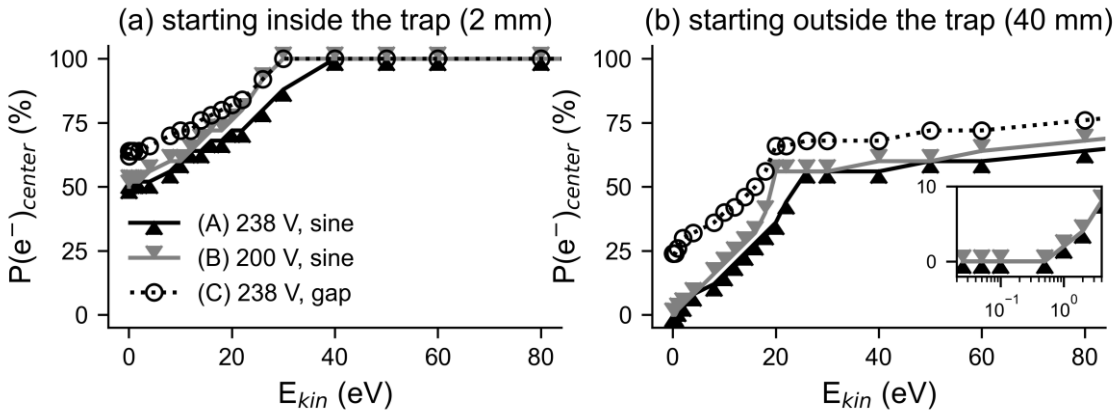

Figure S5. Simulated probability $P(e^-)_{center}$ of electrons to reach the ion trap center along the radial axis (r direction in Figure 7), starting from a distance of (a) 2 mm—relevant for secondary electrons from electron impact ionization in the trap region—or (b) 40 mm from the trap center—representative for electrons from far away, e.g. the cold cathode gauge—as a function of their initial kinetic energy E_{kin}. The inset shows a zoom for low kinetic energies in logarithmic scale. The probability is the fraction of simulated particle trajectories reaching a central sphere of 0.3 mm diameter, sampled over 20 different phases of the oscillating electrode potentials, with an initial velocity vector directed towards the trap center.

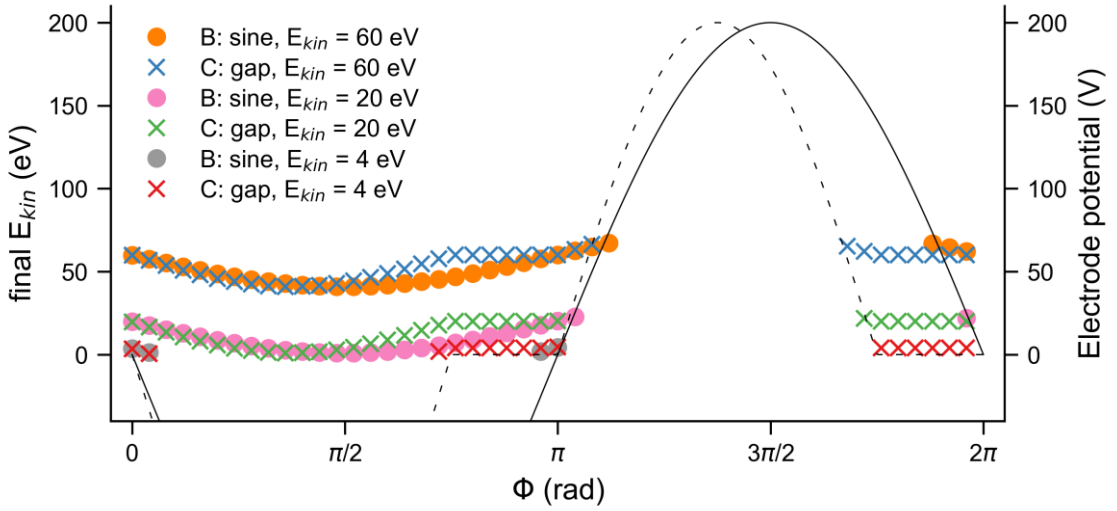

Figure S6. Simulated final kinetic energy of electrons that reach the trap center as a function of the initial phase of the trap waveform (as defined in Figure 7) for electrons starting at a distance of 40 mm from the trap center with 0.025 eV kinetic energy. Data is shown for two waveforms with (B, dots) and without gap (C, crosses). The electrode potentials are drawn as solid and dashed lines, respectively. Slow electrons only reach the trap center in a small range of the period, while gaps in the waveform allow for free electron motion to the trap center without electron acceleration. In the repulsive half cycle, only sufficiently fast electrons are able to reach the trap center.

S6 Different trap settings and low NP charge

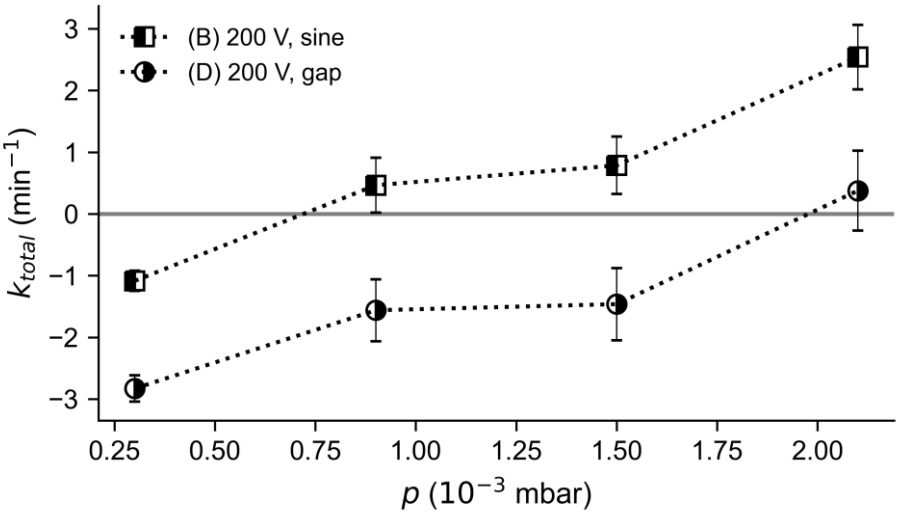

Figure S7. Charging rate k_{total} for Ar gas as a function of pressure p for different trap amplitudes and waveforms B (200 V, sine, as in Figure 8) and D (200 V, sine with gaps) at low NP charges 450–580 e. This shows that even NPs with a low charge can be efficiently discharged using waveform C with gaps.

S7 Analysis of the electron abstraction and attachment contributions

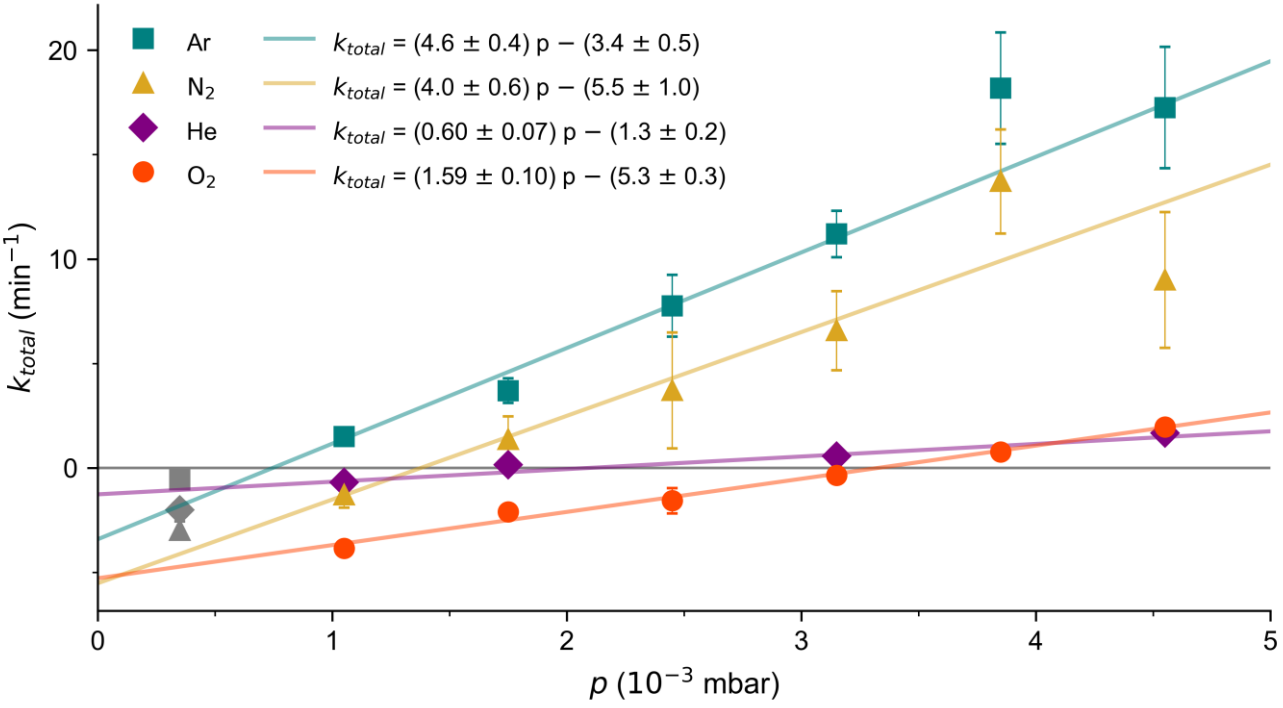

Figure S8. Linear fit (solid lines) of the charging rate k_{total} plotted against pressure p in Figure 5a, for low NP charge (500 to 800 e) and different buffer gases (Ar, N_2, He, O_2) above a pressure of 10^{-3} mbar. Gray data points in the non-linear low pressure regime are excluded from the fit.

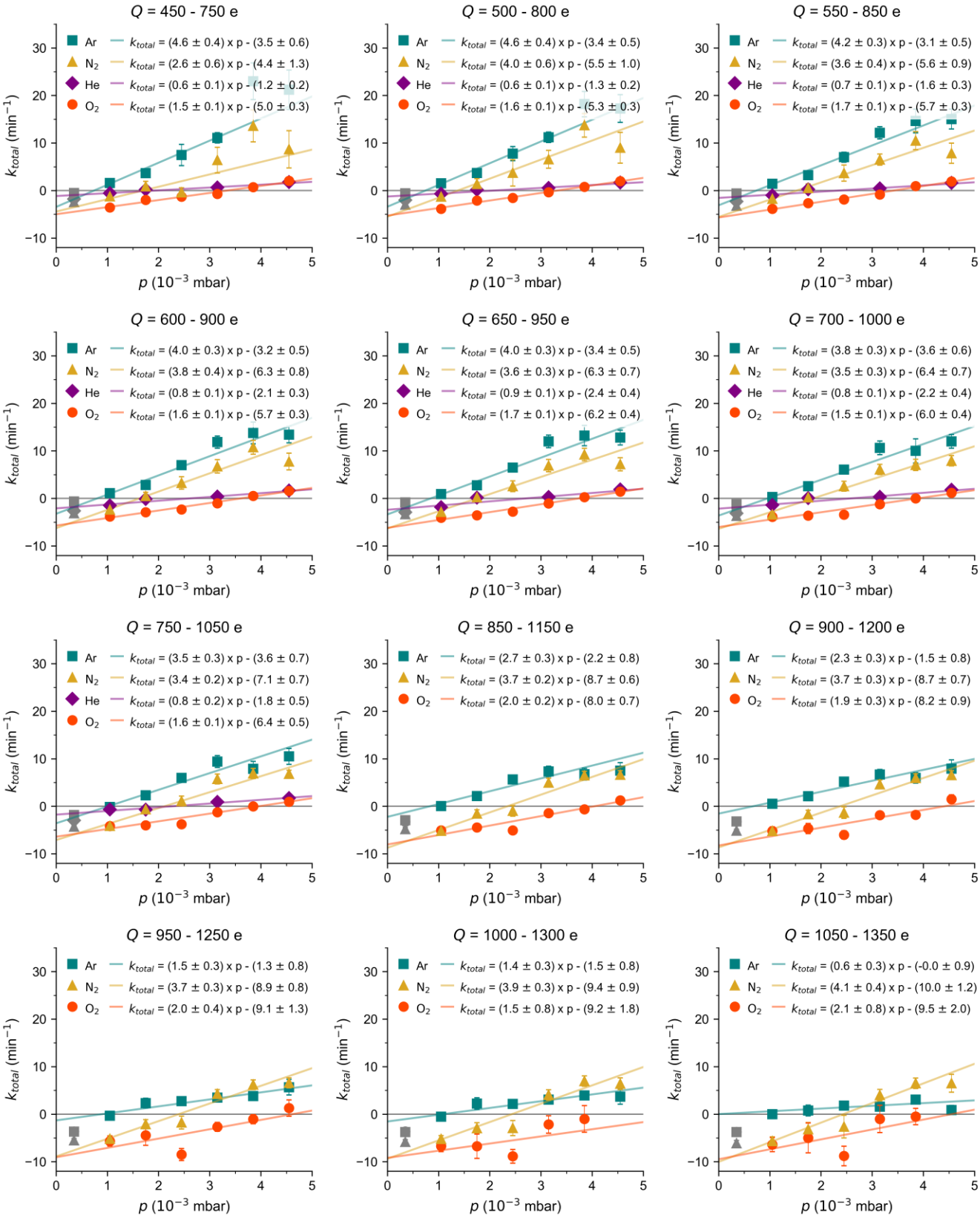

Figure S9. Linear fits (solid lines) of the charging rate $\mathrm{k_{total}} = \mathrm{m\ p} - \mathrm{k_{att}}$ plotted against pressure p for different gases and NP charge Q ranges specified in the plot title.

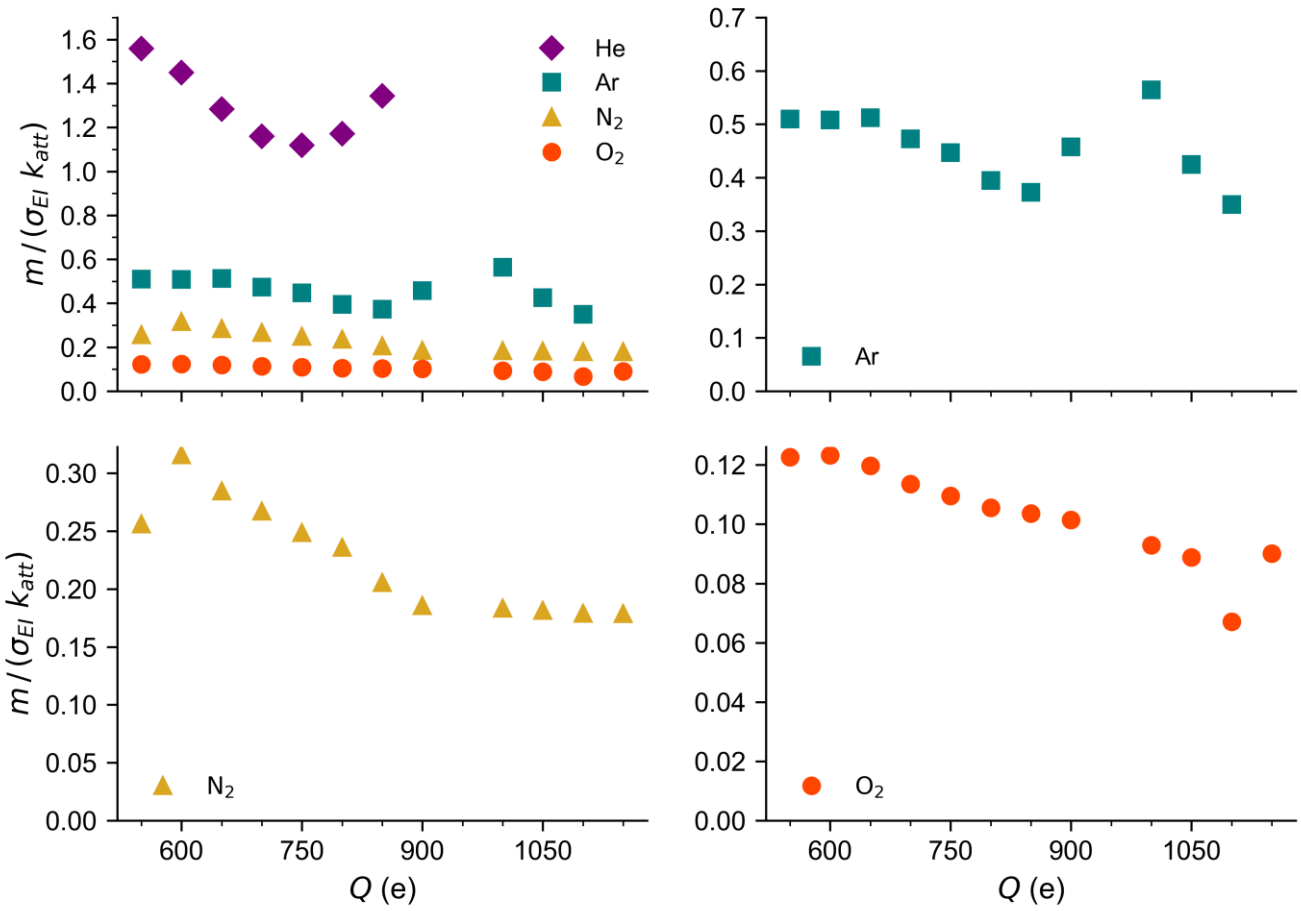

Figure S10. Slope m divided by electron attachment rate $\mathrm{k_{att}}$ (both from Figure S9) and electron impact ionization cross section σ_{EI} (mean for 30–200 eV, see Table 1), in units of µbar^{-1} Å^{-2} and as a function of the NP charge Q with different buffer gases specified in the legends.

S8 Analysis of the charge limit for electron abstraction

To investigate how the electron attachment rate depends on the NP charge, we plotted the $\mathrm{k_{att}}$ values (obtained from the fits of $\mathrm{k_{total}}$ versus p, see Figure S9) along with the total charging rate $\mathrm{k_{total}}$ against the respective mean NP charge $\overline{\mathrm{Q}}$ (see Figure S11). In the following, we attempt to simultaneously fit the data with linear extrapolations such that the dependence of the observed maximum charge $\mathrm{Q_{max}^{total}}$ on the trap potential amplitude $\mathrm{U_0}$ can be roughly reconciled with the relation between $\mathrm{U_0}$ and the maximum charge $\mathrm{Q_{max}^{abstr}}$ given by the energy limit for electron abstraction,

$$\mathrm{Q_{max}^{total}} \approx \mathrm{Q_0} + \mathrm{m_0 U_0} \quad \text{and} \quad \mathrm{Q_{max}^{abst}} = 4\pi\varepsilon_0 \mathrm{R U_0}$$

with the vacuum permittivity ε_0 and NP radius R. To this aim, we relate the linear fit functions for the total charging $\mathrm{k_{total}}$ and electron attachment $\mathrm{k_{att}}$ rates to each other and evaluate the resulting terms for the electron abstraction rate $\mathrm{k_{abst}}$ and maximum charges.

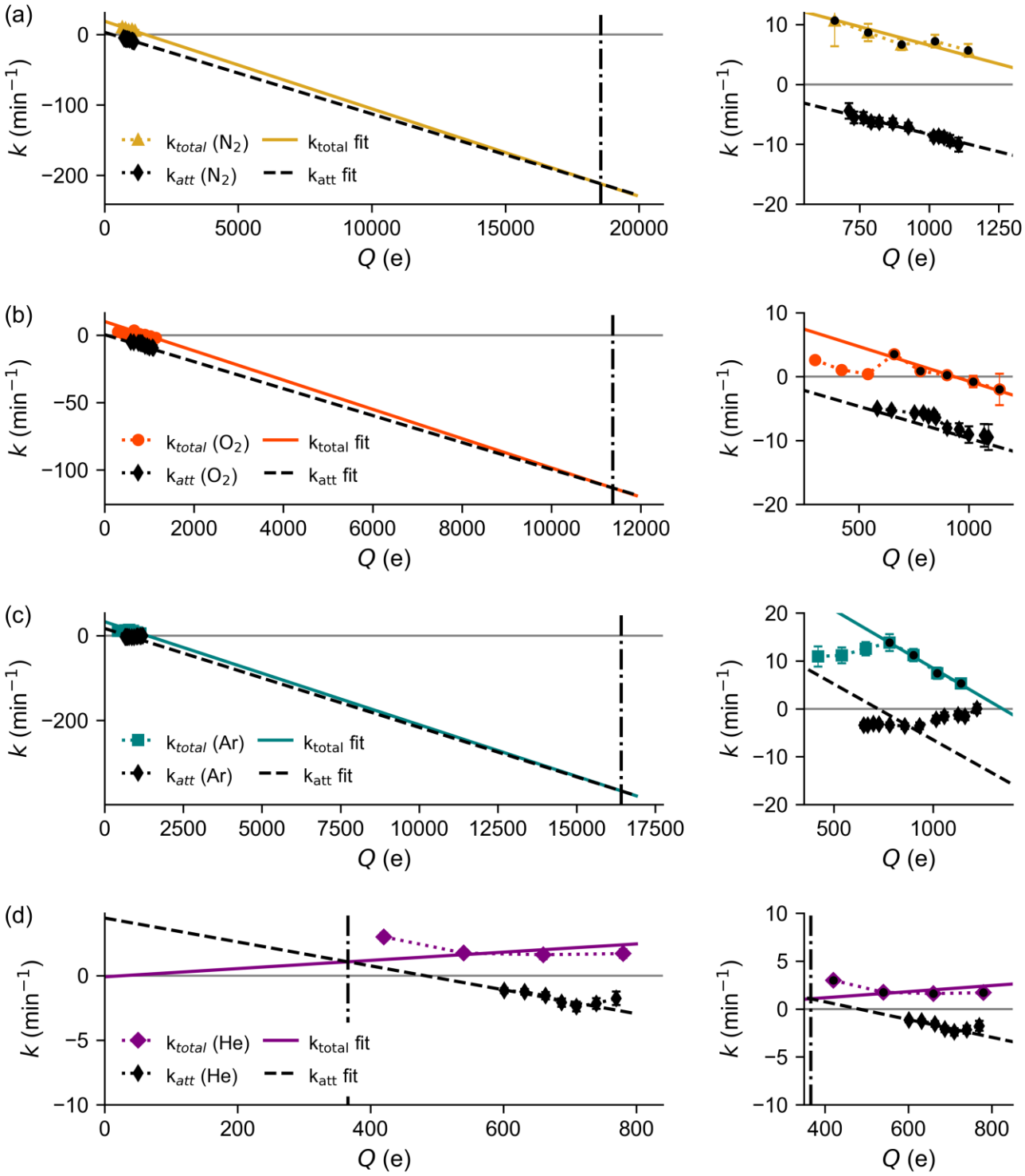

Figure S11. Charging rates $\mathrm{k_{total}}$ and attachment rates $\mathrm{k_{att}}$ with different buffer gases (a) N_2, (b) O_2, (c) Ar and (d) He as a function of the NP charge Q at high pressure (3 x 10^{-3} mbar to 5 x 10^{-3} mbar). For each gas,

the pair of rates is simultaneously fitted (for k_{total} only data marked with a black dot is used for the fit) by two lines with a constraint that is explained in the text. The maximum achievable charge is given by the intersection of k_{total} with the horizontal axis. The maximum charge for electron abstraction is estimated by the intersection $k_{total} = k_{att}$ marked by vertical lines. A zoom into the data region is shown in the right panel for each gas. k_{att} values are obtained from Figure S9.

We define the two linear fit functions

$$k_{total} = k_{abst} - k_{att} = y_1 - m_1 Q$$
$$-k_{att} = y_2 - m_2 Q = \varepsilon\, y_1 - \kappa m_1 Q$$

from which we derive the electron abstraction rate and the following terms for the charge limits corresponding to $k_{abst} = 0$ and $k_{total} = 0$.

$$k_{abst} = (1-\varepsilon)\, y_1 - (1-\kappa)\, m_1 Q$$
$$Q_{max}^{abst} = \frac{(1-\varepsilon)\, y_1}{(1-\kappa)\, m_1} = 4\pi\varepsilon_0 R\, U_0$$
$$Q_{max}^{total} = \frac{y_1}{m_1} = \frac{1-\kappa}{1-\varepsilon} Q_{max}^{abst} = \frac{1-\kappa}{1-\varepsilon} 4\pi\varepsilon_0\, R\, U_0 \approx m_0\, U_0$$

In the last step, we have neglected the intercept Q_0 from the fit in Figure 9 that becomes important at low trap potentials U_0 where electron abstraction is no longer energetically driven by the trap potentials. This omission makes the fit results in Figure S11 inaccurate and forbids a quantitative interpretation thereof. Equating the last two terms gives the relation

$$\varepsilon = 1 - (1-\kappa)\frac{4\pi\varepsilon_0 R}{m_0}$$

which constrains the relation between the dependencies of the different maximum charges on the trap potential amplitude U_0. The free fit variables in Figure S11 are y_1, m_1 and κ. The fit is performed by minimizing the product of the root sum of squared deviations between fit line and data.

S9 Comparison to gold nanoparticles

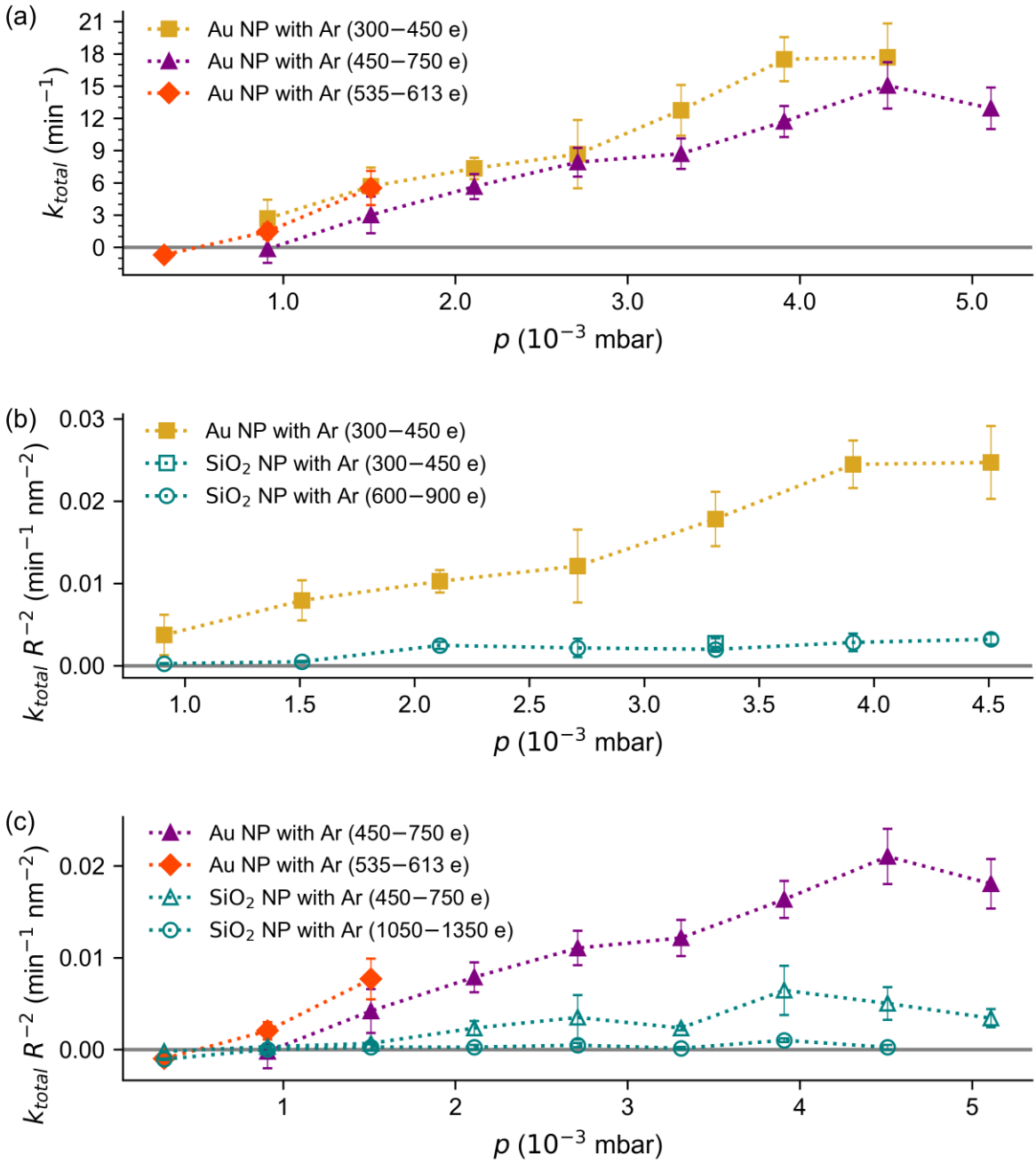

Figure S12. Charging rates k_{total} with Ar buffer gas for Au and SiO_2 NPs plotted against the pressure p at different NP charge Q ranges as specified in the legends. (a) Au data for NP H (red diamonds) and NP J for two different Q ranges (squares and triangles) in Table S1. (b) and (c) charging rates normalized to the squared NP radius to compare Au data for the lower (b) and higher (c) charge range, respectively, to SiO_2 data for the same and doubled charge range, respectively. Charging rates are expected to scale with the geometrical cross section πR^2 which justifies the normalization for comparing different NP sizes. Additionally, the NP surface potential scales with Q/R. Therefore, the Au data with half the NP radius $R/2$ is compared to SiO_2 data at $2Q$, as both factors lead to twice the surface potential $2Q/R$.

S10 Collision cross sections of cations and electrons with a positively charged nanoparticle

A collision of a cation or electron of charge $\pm e$ with the NP occurs if the impact parameter is small enough that the closest distance of approach r_{min} is smaller than the NP radius, $r_{min} < R$. The maximum impact parameter b_{max} that leads to a collision is determined by the condition $r_{min} = R$. The relation between b_{max} and R can be derived from conservation of energy, $\frac{1}{2}mv^2 = \frac{1}{2}mv_R^2 - Q(\pm e) / (4\pi\epsilon_0 R)$, and of angular momentum, $m\, v\, b_{max} = m\, v_R\, R$, with initial velocity v and tangential velocity v_R at the NP surface[2] which is solved for b_{max} and gives the total collision cross section σ_{coll},

$$b_{max} = R\sqrt{1 - \frac{Q\pm e}{4\pi\epsilon_0 R}\frac{1}{\mathrm{E_{kin}}}} \quad \text{and} \quad \sigma_{coll} = \pi\, b_{max}^2 = \pi\, R^2\left(1 - \frac{Q(\pm e)}{4\pi\epsilon_0 R}\frac{1}{\mathrm{E_{kin}}}\right).$$

For cations, σ_{coll} takes its maximum value πR^2 (the geometrical cross section) for $Q = 0$ and σ_{coll} becomes zero when the initial kinetic energy of the cation is smaller than the Coulomb energy at the NP surface. For electrons, the geometrical cross section πR^2 is the minimum value of σ_{coll} when $Q = 0$ and increases with increasing Q or decreasing initial kinetic energy of the electron.

The solution for σ_{coll} is valid in free space without external fields. It breaks down if the range of the collision cross section extends into ion trap regions, where the electric field of the trap electrodes perturbs that of the NP. For a 200 V trap potential, the trap electric field near the trap center builds up with a slope of 28 V mm^{-1} per millimeter distance from the trap center. To estimate the validity range of σ_{coll}, we demand the trap electric field to stay below 1 % of the electric field of the NP at a distance b_{max}. Even for small thermal electron kinetic energy kT at room temperature, and using $R = 65$ nm, this condition is not reached before a very high NP charge $\mathrm{Q} \approx 5 \times 10^6$ e, yielding $b_{max} \approx 0.14$ mm. This value is far beyond $\mathrm{Q} \approx 9000$ e, where σ_{coll} vanishes for cations with $E_{kin} = 200$ eV.

In case of a negatively charged NP, Q has a negative sign and the roles of cations and electrons are reversed. In this case, increasing |Q| leads to a larger collision cross section of a NP with cations due to Coulomb attraction and a smaller collision cross section with electrons due to Coulomb repulsion.

S11 Ionization energy and electron affinity of metal clusters

Following Equation (14) in Ref. 3 and Equation (20) in Ref. 4, we express the energy of a charged spherical cluster with Z excess electrons (and net charge $\mathrm{Q} = -\mathrm{Z\,e}$) in a continuum or liquid drop model in SI units,

$$\mathrm{E(R,Z)} = \mathrm{E(R,0)} - \mathrm{Z}\left(\mathrm{W} + \frac{\mathrm{c}}{\mathrm{R}+\delta}\frac{\mathrm{e}^2}{4\pi\epsilon_0}\right) + \frac{\mathrm{Z}^2}{2(\mathrm{R}+\delta)}\frac{\mathrm{e}^2}{4\pi\epsilon_0},$$

where R is the NP radius, W the bulk work function, c a quantum correction, δ a size-effect coefficient (spill-out factor), e the elementary charge and ϵ_0 the vacuum permittivity. Upon addition of a Z'th electron, the change in energy is

$$\Delta\mathrm{E}(\mathrm{R},\mathrm{Z}) = \mathrm{E}(\mathrm{R},\mathrm{Z}) - \mathrm{E}(\mathrm{R},\mathrm{Z}-1) = -W + \frac{Z - c - \frac{1}{2}}{R+\delta}\frac{e^2}{4\pi\epsilon_0}.$$

Electron attachment is energetically possible as long as $\Delta\mathrm{E}(\mathrm{R},\mathrm{Z})$ remains negative. This condition evaluates to $Z < 4\pi\epsilon_0 e^{-2}(R+\delta)\,W + c + \frac{1}{2} \approx 4\pi\epsilon_0\, e^{-2}\, R\, W$, as the corrections c and δ are negligible for NPs with large radii used in this study.

For an Au NP with $W = 5.1$ eV and 54 nm diameter, the maximum number of excess electrons is $Z \approx 95$. In the special cases $Z = 1$ and $Z = 0$, we obtain the electron affinity $A = -\Delta E(R,1)$ and ionization potential $I = -\Delta E(R,0)$ of a neutral NP, respectively.[3] In case of large charge $+Z$ or $-Z$ and large radius R, the material specific corrections c and δ become negligible. For a NP with large positive charge $Q = -\,Z\,e$, the energy required to remove of another electron is approximately

$$\mathrm{I}(\mathrm{Q}) = -\Delta\mathrm{E}\left(\mathrm{R}, -\frac{Q}{e}\right) \approx \mathrm{W} + \frac{Q\,e}{4\pi\epsilon_0 R},$$

which is the expression used in Equation (3) in the main text.

References

(1) P. W. Atkins and J. de Paula. *Atkins' Physical Chemistry*, 8th ed.; Oxford University Press: Oxford, 2006.

(2) J. E. Allen. Probe Theory – The Orbital Motion Approach. *Phys. Scr.*, 1992, **45**, 497.

(3) J. P. Perdew. Energetics of Charged Metallic Particles: From Atom to Bulk Solid. *Phys. Rev. B*, 1988, **37**, 6175.

(4) M. Seidl, J. P. Perdew, M. Brajczewska and C. Fiolhais. Ionization energy and electron affinity of a metal cluster in the stabilized jellium model: Size effect and charging limit. *J. Chem. Phys.*, 1998, **108**, 8182.